Higher-Layer Identical Partitioning of Integer Set

Chutong Shen†, Yimin D. Zhang†, and Shunqiao Sun‡

† Department of Electrical and Computer Engineering, Temple University, Philadelphia, PA 19122, USA

‡ Department of Electrical and Computer Engineering, The University of Alabama, Tuscaloosa, AL 35487, USA

***Abstract*—Partitioning a set of consecutive integers into multiple identical subsets with consecutive lags offers an effective strategy for enabling multiple radars to share time and spectrum resources, thereby improving spectrum utilization. While previous studies focuses on one- or two-layer partitioning schemes, this paper extends these approaches to higher-layer identical partitioning schemes. The goal is to increase the number of subsets while maintaining a high count of consecutive lags within each subset. The paper provides an analysis of the resulting lag structures and formulates the optimization of partitioning parameters. A dimension-ordering strategy is proposed to maximize the number of consecutive lags achievable by each subarray. Additionally, practical design guidelines are developed to facilitate an efficient search for optimal partitioning solutions.**

***Index Terms*—Integer set partitioning, sparse arrays, sparse waveform design, spectrum sharing, radar signal processing.**

I. INTRODUCTION

Sparse array designs have become increasingly attractive in modern radar and sonar systems as well as wireless communications since they allow for enhanced spatial resolution and interference reduction capability with fewer physical sensors [1]–[4]. Uniform linear arrays (ULAs) used in traditional systems face severe restrictions on the achievable degrees of freedom (DOFs) and suffer from mutual coupling effects that negatively impact the performance of direction-of-arrival (DOA) estimation and adaptive beamforming [5]. The development of structured sparse arrays, such as nested arrays [6]–[10], coprime arrays [11]–[16], and maximum inter-element spacing constraint (MISC) arrays [17]–[19], provide effective solutions to these technical issues. In particular, the use of the difference coarray concept enables achieving $\mathcal{O}(N^2)$ DOFs from N physical sensors. Modern sensing and communication applications greatly benefit from sparse sensor arrays and the accompanies sparse signal processing techniques as a result of increased array aperture, enhanced DOFs, and high design flexibility [20].

Advancements in sparse array design and processing have also inspired analogous approaches in radar waveform design. For single-target or single-signal scenarios, a small number of sinusoidal signals with mutually coprime frequencies can enable unambiguous frequency and range estimation by leveraging the Chinese Remainder Theorem [21], [22]. Similarly, structured array designs based on difference coarrays have influenced sparse waveform design, motivating the use of thinned discrete frequencies and pulse patterns for target range and Doppler estimation [23]–[27]. These sparse waveforms consume fewer time and frequency resources, providing efficient solutions to mitigate spectrum congestion as the number of sensing platforms continues to grow.

Nevertheless, existing techniques only considered the sparse array and waveform design for a single sensing platform. Recently, the identical partitioning method introduced in [28] provides a general framework that enables multiple sensing platforms to fairly share spatial, temporal, and/or spectral resources through sparse arrays and waveforms in an interference-free manner. An extension of this concept, referred to as identical division, is presented in [29]. The key distinction between identical partitioning and identical division is that the former requires every element in the original consecutive integer set to be used exactly once, whereas the latter allows some elements to remain unused.

In the above studies, nested configurations naturally divide a one-dimensional (1D) set into two mirrored sparse subsets, and their extension to two-dimensional (2D) as well as two-layer architectures enables the generation of four identical subsets. Building on this foundation, this paper extends the concept to higher-layer identical partitioning schemes that create a larger number of identical subsets and thus reduces the redundancy in the rendered difference lags. The goal is to increase the number of subsets while maintaining a high count of consecutive lags within each subset. Another novel contribution of this paper is the analysis of the resulting lag structures and the optimization of partitioning parameters. We also develop a dimension-ordering strategy to maximize the number of consecutive lags achievable by each subarray. Additionally, practical design guidelines are provided to facilitate the efficient search for optimal partitioning solutions.

The remainder of this paper is structured as follows: Section II reviews the fundamentals of the existing single- and two-layer partitioning schemes. Section III presents the mathematical model and methodology for three-layer partitioning as well as a partition search method. Section IV provides simulation results of the three-layer partitioning scheme and its application to sparse waveform design for target range estimation. The performance is compared to the two-layer partitioning counterpart to verify the effectiveness of the three-layer partitioning scheme. Section V concludes this paper.

Notations: We use lower-case (upper-case) bold characters to denote vectors (matrices). $(\cdot)^{\mathrm{T}}$ denotes the vector transpose, and $\mathrm{vec}(\cdot)$ represents the vectorization operation. $|\mathbb{Q}|$ denotes

C. Shen and Y. D. Zhang are supported in part by the National Science Foundation (NSF) under Grant ECCS-2236023. S. Sun is supported in part by NSF under Grants CCF-2153386 and ECCS-2033433.

the cardinality of set $\mathbb{Q}$, and $\cup$ denotes the union operator. $\otimes$ and $\circ$ denote the Kronecker product and generalized outer product, respectively.

II. Identical Partitioning of Integer Set

A. Single-Layer Partitioning

We begin with a brief review of the concept of 1D single-layer two-subset partitioning scheme, where a consecutive integer set is partitioned to two nested subsets [28]. The two subsets are identical (after rotation and shifting), and provide the same consecutive difference lags.

An ordered integer set consisting of M consecutive integers, $\mathbb{Q} = \{1, 2, \ldots, M\}$, is divided into two non-overlapping subsets, $\mathbb{Q}_1$ and $\mathbb{Q}_2$, such that

$$\mathbb{Q} = \mathbb{Q}_1 \cup \mathbb{Q}_2, \tag{1}$$

where $\mathbb{Q}_1$ and $\mathbb{Q}_2$ adopt a nested structure. We assume that $M \geq 6$ is an even integer. The first subset $\mathbb{Q}_1$, which consists of two consecutive elements, 1 and 2, forms the inner group, whereas the outer group comprises an evenly spaced selection of elements separated by an interval of 2. Denoting $N = (M-4)/2$ as the number of elements in the outer group, the locations of the $|\mathbb{Q}_1| = N + 2$ elements are given as

$$\mathbb{Q}_1 = \{1, 2, 4, 6, \ldots, 2N, 2N + 2\}. \tag{2}$$

Similarly, the second subset $\mathbb{Q}_2$ consists of the same number of $N + 2$ elements located at

$$\mathbb{Q}_2 = \{3, 5, 7, \ldots, 2N - 1, 2N + 1, 2N + 3, 2N + 4\}. \tag{3}$$

Both subsets inherit consecutive difference lags ranging from $-2N-1$ to $2N+1$. As such, any consecutive integer set with an even number of elements can be systematically partitioned into two nested subsets.

For notation convenience, we define the following $M \times 1$ masking vectors

$$\mathbf{m}_g(k) = \begin{cases} 1, & \text{if } k \in \mathbb{Q}_g, \\ 0, & \text{if } k \notin \mathbb{Q}_g, \end{cases} \tag{4}$$

with $g = 1, 2$ for subsets $\mathbb{Q}_1$ and $\mathbb{Q}_2$.

B. Two-Dimensional Partitioning

The 1D single-layer partitioning scheme is extended to a 2D setting by extending the nested construction independently in two directions, denoted as x and y. Consider a 2D integer set $\mathbb{Q} = \mathbb{Q}^{[1]} \times \mathbb{Q}^{[2]}$ with sizes $|\mathbb{Q}^{[1]}| = M^{[1]} = 2N^{[1]} + 4$ and $|\mathbb{Q}^{[2]}| = M^{[2]} = 2N^{[2]} + 4$ in the respective dimensions. In each dimension, $\mathbb{Q}^{[i]}$ is partitioned following the same procedure as described in Section II A for $i = 1, 2$. In this case, the mask can be represented as a matrix, given as

$$\mathbf{M}_{g_1,g_2} = \mathbf{m}^{[1]}_{g_1} \left(\mathbf{m}^{[2]}_{g_2}\right)^{\mathrm{T}}, \tag{5}$$

where $g_1 \in \{1, 2\}$ and $g_2 \in \{1, 2\}$. As such, we obtain four identically partitioned 2D subsets.

C. Two-Layer Partitioning

Vectorizing the 2D subsets forms a structured two-layer configuration. Vectorization of $\mathbf{M}_{g_1,g_2}$ yields an $M^{[1]}M^{[2]} \times 1$ vector

$$\tilde{\mathbf{m}}_{g_1,g_2} = \mathrm{vec}(\mathbf{M}_{g_1,g_2}) = \mathbf{m}^{[2]}_{g_2} \otimes \mathbf{m}^{[1]}_{g_1} \tag{6}$$

for $g_1 \in \{1, 2\}$ and $g_2 \in \{1, 2\}$. As such, we obtain four subsets of 1D two-layer super-nested partitioning from a 1D consecutive integer set.

III. Three-Layer Partitioning

The two-layer partitioning scheme discussed in the previous section provides a structured way to form four subsets by combining two 1D nested sequences along two orthogonal directions. While the effectiveness of this approach and its identical division variation has been demonstrated in [28]–[30], the two-layer structure offers limited flexibility in further dividing resources, rendering it less effective, particularly when the integer set is large. To enable a greater number of subsets and introduce design flexibility, we extend the hierarchical formulation to higher-layer configurations.

In this section, we describe the formulation of a three-layer framework that generalizes nested partitioning to support a scalable and structured decomposition. In the next section, we present its optimization and discuss its further extension to a four-layer partitioning scheme.

A. Three-Dimensional Partitioning

We first consider a three-dimensional (3D) partitioning scheme as an extension of the 2D counterpart. Define a 3D integer set $\mathbb{Q} = \mathbb{Q}^{[1]} \times \mathbb{Q}^{[2]} \times \mathbb{Q}^{[3]}$ with dimensions $M^{[1]} = 2N^{[1]} + 4$, $M^{[2]} = 2N^{[2]} + 4$, and $M^{[3]} = 2N^{[3]} + 4$ respectively along the x-, y-, and z-directions. Define the g-th nested subset in the x-, y- and z-directions as $\mathbb{Q}^{[1]}_g$, $\mathbb{Q}^{[2]}_g$, and $\mathbb{Q}^{[3]}_g$, respectively, each specified by a binary mask defined as

$$\mathbf{m}^{[\eta]}_g(k) = \begin{cases} 1, & \text{if } k \in \mathbb{Q}^{[\eta]}_g, \\ 0, & \text{if } k \notin \mathbb{Q}^{[\eta]}_g \end{cases} \tag{7}$$

for $\eta \in \{1, 2, 3\}$ and $g \in \{1, 2\}$.

By taking the outer product of $\mathbf{m}^{[1]}_g$, $\mathbf{m}^{[2]}_g$, and $\mathbf{m}^{[3]}_g$, we obtain 8 identical 3D subsets. The corresponding mask tensor is given as

$$\mathcal{M}_{g_1,g_2,g_3} = \mathbf{m}^{[1]}_{g_1} \circ \mathbf{m}^{[2]}_{g_2} \circ \mathbf{m}^{[3]}_{g_3}, \tag{8}$$

where $g_1, g_2, g_3 \in \{1, 2\}$. An example is shown in Fig. 1 for the case of $N^{[1]} = 2$, $N^{[2]} = 1$, and $N^{[3]} = 1$.

B. Three-Layer Super-Nested Partitioning

To obtain 1D super-nested partitioning scheme from the 3D partitioning results, the tensor $\mathcal{M}_{g_1,g_2,g_3}$ is vectorized as

$$\tilde{\mathbf{m}}_{g_1,g_2,g_3} = \mathrm{vec}(\mathcal{M}_{g_1,g_2,g_3}) = \mathbf{m}^{[3]}_{g_3} \otimes \mathbf{m}^{[2]}_{g_2} \otimes \mathbf{m}^{[1]}_{g_1}. \tag{9}$$

We refer to this as three-layer super-bested partitioning of a 1D consecutive integer set. It is noted that, considering that $N^{[1]} \geq 1$, $N^{[2]} \geq 1$, and $N^{[3]} \geq 1$, the minimum number of elements in the original consecutive integer set is 216.

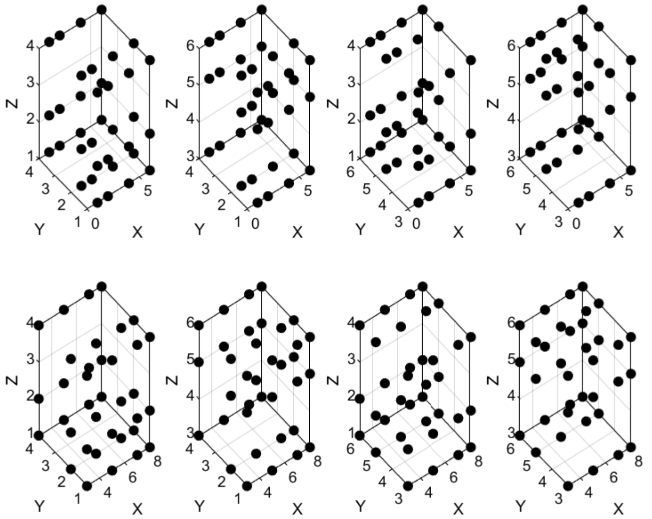

Fig. 1: Example of 3-D partitioned subsets with $N^{[1]} = 2$, $N^{[2]} = 1$, and $N^{[3]} = 1$. Black dots indicate present elements.

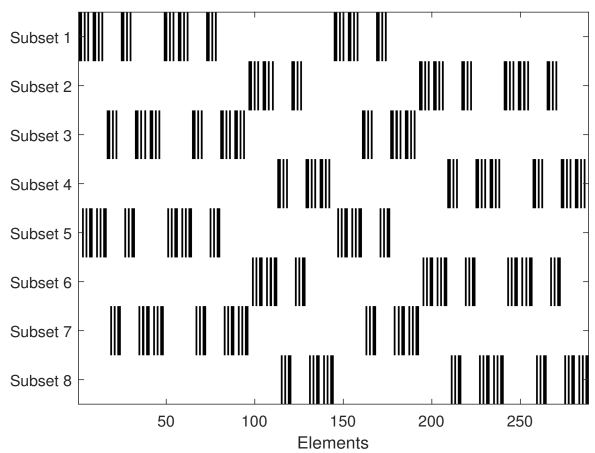

Fig. 2: Example of eight 1D subsets obtained from 3-layer partitioning. Black lines indicate the positions of present elements.

C. Optimized Three-Layer Partitioning

To analyze the performance of the three-layer structure under fixed total element constraints, we derive the relationship between layer dimensions and the resulting resolution. In particular, we focus on the maximum consecutive difference lag $L_{\max}$, which serves as a key measure of the achievable resolution.

The three-layer super-nested partitioning scheme extends nested partitioning to construct eight subsets as illustrated in Fig. 2. The total number of elements in the full set is given by

$$M = (2N^{[1]} + 4)(2N^{[2]} + 4)(2N^{[3]} + 4). \tag{10}$$

The number of elements in each subset is

$$M_{\text{subset}} = (N^{[1]} + 2)(N^{[2]} + 2)(N^{[3]} + 2), \tag{11}$$

and the number of the resulting maximum consecutive difference lags is

$$L_{\max} = (2N^{[1]} + 4)\left[(2N^{[2]} + 4)(2N^{[3]} + 1) + (2N^{[2]} + 1)\right] + (2N^{[1]} + 1). \tag{12}$$

Since $N^{[1]}, N^{[2]}, N^{[3]}$ are discrete variables, we quantify their impact on $L_{\max}$ using forward finite differences. The difference represents the change in $L_{\max}$ when a specific $N^{[i]}$ with $i \in \{1, 2, 3\}$ is incremented by 1 while keeping the other two fixed. The differences due to a unit change in these three indices are respectively given by:

$$\Delta L_{\max}^{[1]} = 8N^{[2]}N^{[3]} + 8N^{[2]} + 16N^{[3]} + 12, \tag{13}$$

$$\Delta L_{\max}^{[2]} = 8N^{[1]}N^{[3]} + 8N^{[1]} + 16N^{[3]} + 16, \tag{14}$$

$$\Delta L_{\max}^{[3]} = 8N^{[1]}N^{[2]} + 16N^{[1]} + 16N^{[2]} + 32. \tag{15}$$

The constant term in $\Delta L_{\max}^{[3]}$ is 32, which is the largest among all three forward finite difference results. This indicates that, for any reference pair of $N^{[i]}$, incrementing $N^{[3]}$ alone yields the fastest increase in $L_{\max}$. Additionally, the linear coefficients associated with $N^{[1]}$ and $N^{[2]}$ in $\Delta L_{\max}^{[3]}$ are 16, which are twice as large as the corresponding coefficients 8 in $\Delta L_{\max}^{[1]}$ and $\Delta L_{\max}^{[2]}$. This amplifies the sensitivity of $L_{\max}$ to changes in $N^{[3]}$ compared to $N^{[1]}$ and $N^{[2]}$. Similarly, applying the same comparison between $\Delta L_{\max}^{[2]}$ and $\Delta L_{\max}^{[1]}$, we observe that $\Delta L_{\max}^{[2]}$ has a larger constant term than $\Delta L_{\max}^{[1]}$, making it more sensitive to the unit increment.

Therefore, we can observe from the above analysis that, when $N^{[1]} \leq N^{[2]} \leq N^{[3]}$, $L_{\max}$ reaches its maximum value. Table I presents the case where the total number of elements M is set to 2160, along with all corresponding $N^{[i]}$ values that satisfy this constraint. From the table, we observe that the configuration $(N^{[1]}, N^{[2]}, N^{[3]}) = (1, 1, 28)$ yields the highest $L_{\max} = 2073$. This aligns with the theoretical insight that allocating a larger value to $N^{[3]}$ is beneficial, as the third layer has the highest impact on $L_{\max}$. Other top configurations such as $(1, 3, 16)$ and $(1, 4, 13)$ also follow the pattern $N^{[1]} \leq N^{[2]} \leq N^{[3]}$, ensuring that $N^{[3]}$ is prioritized, but because they do not maximize $N^{[3]}$, their resulting $L_{\max}$ will is slightly lower than that of the top choice. Comparatively, configurations where $N^{[1]}$ or $N^{[2]}$ becomes larger, such as $(4, 1, 13)$ or $(1, 7, 8)$, also lead to a reduced $L_{\max}$. We also plot the difference lags for several representative configurations in Fig. 3, which agree with the above discussion. This observation further reinforces the conclusion that maximizing $N^{[3]}$ while maintaining a non-decreasing ordering across $N^{[1]}$, $N^{[2]}$, and $N^{[3]}$ is an effective strategies to optimize the maximum consecutive lags.

D. Constraint-Based Partition Search Method

We propose a method that, given the total number of elements M, efficiently determines the optimal three-layer partitioning. We apply a constraint-based partition search method to reduce the search space. It begins by enumerating candidate values of $M^{[1]}$ (e.g., 6, 8, 10, ...) in ascending order.

TABLE I: All $(N^{[1]}, N^{[2]}, N^{[3]})$ Combinations for $M = 2160$ and the Corresponding $L_{\max}$ Values

$(N^{[1]}, N^{[2]}, N^{[3]})$	$L_{\max}$	$(N^{[1]}, N^{[2]}, N^{[3]})$	$L_{\max}$
(1, 1, 28)	2 073	(3, 7, 4)	1 777
(1, 3, 16)	2 025	(7, 3, 4)	1 761
(3, 1, 16)	2 017	(13, 1, 4)	1 737
(1, 4, 13)	2 001	(1, 16, 3)	1 713
(4, 1, 13)	1 989	(4, 7, 3)	1 701
(1, 7, 8)	1 929	(7, 4, 3)	1 689
(1, 8, 7)	1 905	(16, 1, 3)	1 653
(7, 1, 8)	1 905	(4, 13, 1)	1 413
(3, 4, 7)	1 897	(7, 8, 1)	1 401
(4, 3, 7)	1 893	(8, 7, 1)	1 397
(8, 1, 7)	1 877	(28, 1, 1)	1 317
(1, 13, 4)	1 785		

For each candidate, we check whether $M \bmod M^{[1]} = 0$, ensuring that the total element count is divisible by $M^{[1]}$, and whether the resulting quotient $M/M^{[1]}$ is divisible by 4, i.e., $(M/M^{[1]}) \bmod 4 = 0$, so that it can be split into even $M^{[2]}$ and $M^{[3]}$ values. If either condition fails, the candidate is discarded.

Consider an example where $M = 10000$. When $M^{[1]} = 8$, we obtain $M/M^{[1]} = 1250$, which is even but is not divisible by 4. Thus, this configuration is rejected. Instead, when we choose $M^{[1]} = 10$, the resulting $M/M^{[1]} = 1000$, which is divisible by 4 and is therefore acceptable. Following the constraint $N^{[1]} \leq N^{[2]}$, we select the smallest feasible $M^{[2]} = 10$, yielding the final configuration as $(M^{[1]}, M^{[2]}, M^{[3]}) = (10, 10, 100)$. This partition search method eliminates invalid configurations early and significantly reduces the brute-force complexity from $\mathcal{O}(M)$ to $\mathcal{O}(\sqrt{M})$, while ensuring balanced and valid three-layer allocations.

E. Extension to Higher Layers

The same partition search method used in three-layer partitioning can be extended to higher layers, while maintaining balanced subset allocation and computational efficiency. In general, an M-element consecutive integer set $\mathbb{Q}$ can be partitioned into 2^K subsets in a K-layer partitioning scheme, provided that $(M \mod 2^K) = 0$. To ensure feasible partitioning, the minimum total number of elements M required for a K-layer partitioning structure is given by $M_{\min} = 6^K$. For instance, three-layer partitioning requires at least 216 elements, while four-layer partitioning requires at least 1296 elements.

It is also noted that the practical advantage of adopting a K-layer partitioning over a lower-layer structure becomes significant only when M is sufficiently large. If M is equal or only slightly exceed 6^K, $L_{\max}$ offered by a K-layer partitioning is smaller than that offered by a $(K-1)$-layer counterpart. For example, when $M = 216$, a two-layer configuration with $(N^{[1]}, N^{[2]}) = (1, 16)$ provides $L_{\max} = 201$, while the corresponding three-layer configuration $(N^{[1]}, N^{[2]}, N^{[3]}) = (1, 1, 1)$ provides $L_{\max} = 129$, with the three-layer structure generating eight subsets compared to four in the two-layer case. Thus, it diminishes spectral diversity and degrades performance. Therefore, meaningful benefits of K-layer structures emerge when M is considerably larger than 6^K, allowing for a sufficient number of subsets to 2^K compared to 2^{K-1} while keeping performance acceptable, as illustrated through numerical examples in Section IV.

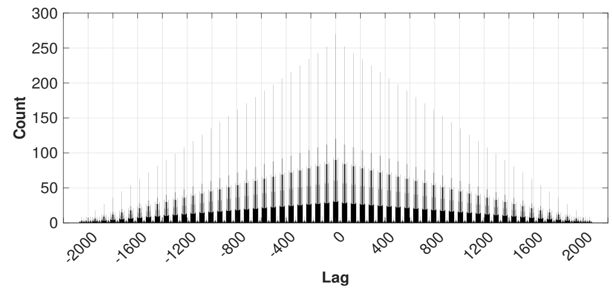

(a) $(N^{[1]}, N^{[2]}, N^{[3]}) = (1, 1, 28)$, $L_{\max} = 2073$

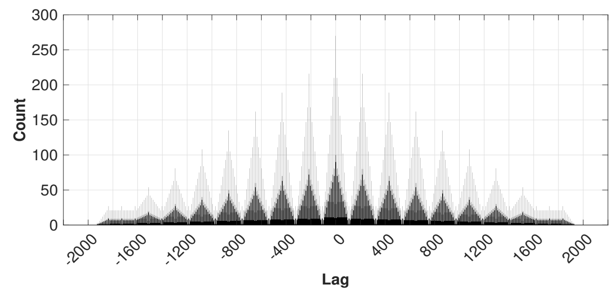

(b) $(N^{[1]}, N^{[2]}, N^{[3]}) = (1, 7, 8)$, $L_{\max} = 1929$

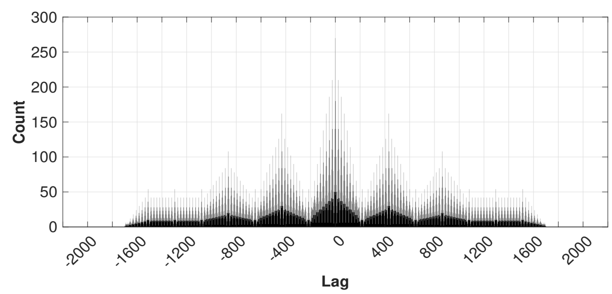

(c) $(N^{[1]}, N^{[2]}, N^{[3]}) = (4, 7, 3)$, $L_{\max} = 1701$

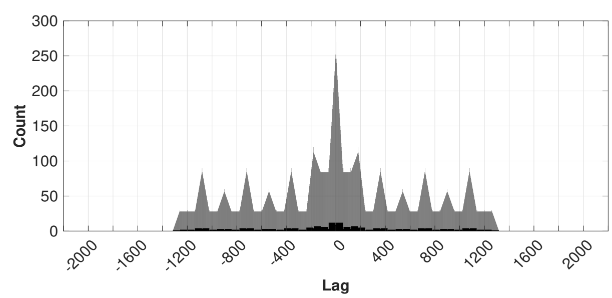

(d) $(N^{[1]}, N^{[2]}, N^{[3]}) = (28, 1, 1)$, $L_{\max} = 1317$

Fig. 3: Lag plots for different $(N^{[1]}, N^{[2]}, N^{[3]})$ combinations.

IV. Simulation Results

In this section, we consider a step-frequency radar model that partitions the available bandwidth into multiple non-

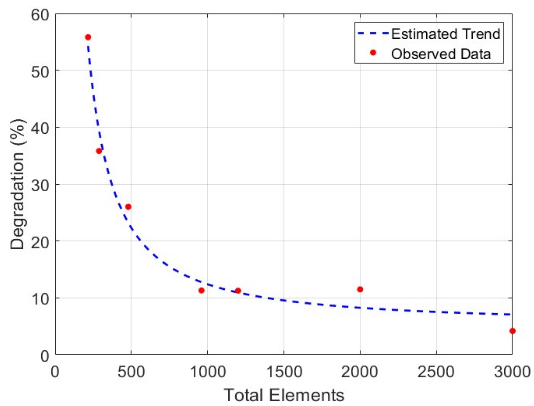

Fig. 4: Degradation trend versus the number of elements.

overlapping step-frequency subsets, allowing multiple radar units to operate simultaneously without mutual interference [28].

A step-frequency radar uses an equally spaced step-frequency waveform, where the available bandwidth B is divided into N_f frequency bins with a step-frequency

$$f_\Delta = \frac{B}{N_f}. \tag{16}$$

As such, each transmitted pulse corresponds to a discrete frequency index l with center frequency $f_l = f_0 + (l-1)f_\Delta$ for $k = 1, \cdots, N_f$.

When all the step frequency bins are used by a single radar, the synthetic range resolution obtained by coherently processing the return signal from a target corresponding to these N_f pulses is given as

$$\Delta R = \frac{c}{2B}, \tag{17}$$

and the maximum unambiguous range is

$$R_{\max} = \frac{c}{2f_\Delta}, \tag{18}$$

where $c = 3 \times 10^8$ m/s is the speed of electromagnetic waves.

When identical partitioning is applied, the N_f frequency bins are assigned to multiple radars. Denote $\mathbb{Q} = \{1, \cdots, N_f\}$ and assume that $|\mathbb{Q}| = N_f \geq 6^K$ is divisible by 2^K, we can form 2^K identically partitioned subsets, each to a radar, i.e., the i-th radar uses frequency bins with indices $k \in \mathbb{Q}_i$.

As such, the maximum number of consecutive difference lags $L_{\max}$ determines the number of consecutive frequency bins and, subsequently, the effective bandwidth of each subset is given as

$$B_{\text{subset}} = L_{\max} f_\Delta, \tag{19}$$

which directly determines the radar's range resolution.

For simulation, we consider a full bandwidth of $B = 1.5$ GHz, divided into $N_f = 3000$ frequency bins, rendering in a step frequency of $f_\Delta = 0.5$ MHz. For single-radar operation, the full bandwidth provides a range resolution of $\Delta R = 0.1$ m and a maximum unambiguous range of $R_{\max} = 300$ m.

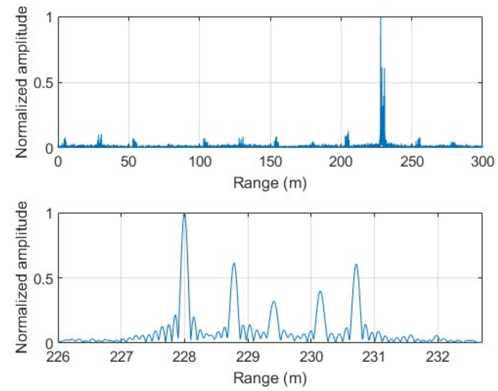

(a) Two-layer partitioning

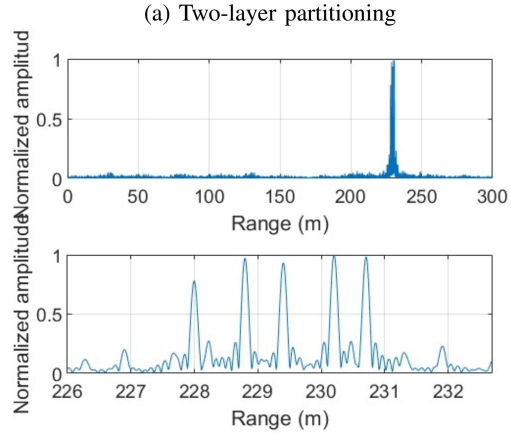

(b) Three-layer partitioning

Fig. 5: Performance of two-layer and three-layer.

Under two-layer partitioning, the frequency bins are divided into four identical subsets, each containing 750 frequency bins. The optimal configuration with $N^{[1]} = 1$ and $N^{[2]} = 248$ yields $L_{\max} = 2985$, which corresponds to only a 0.5% reduction relative to exclusive single-radar use. In this case, each radar attains an effective bandwidth of $B_{\text{subset}} = L_{\max} f_\Delta = 1492.5$ MHz obtained from the correlation lags, and the corresponding range resolution is $\Delta R_{\text{subset}} = 0.1005$ m.

When three-layer partitioning is applied, the same spectrum can support eight radars, each assigned 350 frequency bins. In this case, the optimal configuration with $N^{[1]} = 1$, $N^{[2]} = 3$, and $N^{[3]} = 23$ yields a maximum lag span of $L_{\max} = 2865$ frequency bins. This corresponds to a 4.5% reduction relative to single-radar use and about a 4.0% reduction compared

TABLE II: Two- and Three-Layer Partitioning: Number of Frequency Bins versus Range-Resolution Degradation

N_f	**Two-layer**	**Three-Layer**	**Degradation**
216	1.4925 m	2.3256 m	55.82%
288	1.0989 m	1.4925 m	35.82%
480	0.6452 m	0.8130 m	26.01%
960	0.3175 m	0.3534 m	11.31%
1200	0.2532 m	0.2817 m	11.26%
2000	0.1514 m	0.1688 m	11.49%
3000	0.1005 m	0.1047 m	4.18%

with the two-layer partitioning case. The resulting effective bandwidth is $B_{\text{subset}} = 1432.5$ MHz, leading to a range resolution of 0.1047 m.

Table II compares the range resolution between two-layer and three-layer partitioning, assuming optimal parameter selection in both cases. The degradation ratio against the value of N_f is plotted in Fig. 4. To visualize the asymptotic trend, a curve fitted via nonlinear least squares regression using a power function model is included. The loss decreases rapidly as N_f increases, confirming that three-layer structures become increasingly efficient for large-scale array deployments.

To demonstrate the range estimation performance in a challenging multi-target scene, we consider five closely spaced targets whose separations are randomly distributed between 0.5 m and 0.8 m. The radar systems with both the two- and three-layer partitioning schemes operate with the same step frequency and maximum unambiguous range. As shown in Fig. 5, where the targets are located at $\{228.0,\ 228.8,\ 229.4,\ 230.2,\ 230.7\}$ m, both partitioning schemes successfully resolve the five distinct peaks despite the close spacing. Although the three-layer partitioning theoretically yields a slightly coarser resolution, the observed degradation is nearly negligible. This confirms that the three-layer structure effectively doubles the number of available subsets, thus supporting more simultaneous radar operations while maintaining high-resolution performance comparable to the two-layer counterpart.

V. CONCLUSION

This paper introduced a three-layer super-nested subset partitioning framework that generalizes single- and two-layer partitioning schemes. We derived optimal parameter selections to maximize the lag span for each subset, providing guidance for efficient resource allocation under a constrained total element count. To address computational challenges, a partition search method was implemented to systematically reduce the search space. Simulation results quantified the performance degradation of the three-layer structure and show that, for large-size integer sets, the degradation is negligible, while enabling a greater number of radars to operate simultaneously without interference.

REFERENCES

[1] A. Moffet, "Minimum-redundancy linear arrays," *IEEE Transactions on Antennas and Propagation*, vol. 16, no. 2, pp. 172–175, 1968.

[2] R. T. Hector and S. A. Kassam, "The unifying role of the co-array in aperture synthesis for coherent and incoherent imaging," *Proceedings of the IEEE*, vol. 78, no. 4, pp. 735–752, 1990.

[3] Y. Gu, N. A. Goodman, and Y. D. Zhang, "Adaptive beamforming via sparsity-based reconstruction of covariance matrix," in *Compressed Sensing in Radar Signal Processing*, A. D. Maio, Y. C. Eldar, and A. Haimovich, Eds. Cambridge University Press, 2019.

[4] C. Zhou, Y. Gu, Y. D. Zhang, and Z. Shi, "Sparse array interpolation for direction-of-arrival estimation," in *Sparse Arrays for Radar, Sonar, and Communications*, M. G. Amin, Ed. Wiley-IEEE Press, 2024.

[5] H. L. V. Trees, *Optimum Array Processing: Part IV of Detection, Estimation, and Modulation Theory*. New York, NY: Wiley, 2002.

[6] P. Pal and P. P. Vaidyanathan, "Nested arrays: A novel approach to array processing with enhanced degrees of freedom," *IEEE Transactions on Signal Processing*, vol. 58, no. 8, pp. 4167–4181, 2010.

[7] A. Ahmed, Y. D. Zhang, and B. Himed, "Effective nested array design for fourth-order cumulant-based DOA estimation," in *Proceedings of IEEE Radar Conference*, 2017, pp. 998–1002.

[8] J. Liu, Y. Zhang, Y. Lu, S. Ren, and S. Cao, "Augmented nested arrays with enhanced DOF and reduced mutual coupling," *IEEE Transactions on Signal Processing*, vol. 65, no. 21, pp. 5549–5563, 2017.

[9] C.-L. Liu and P. P. Vaidyanathan, "Super nested arrays: Linear sparse arrays with reduced mutual coupling—part I: Fundamentals," *IEEE Transactions on Signal Processing*, vol. 64, no. 15, pp. 3997–4012, 2016.

[10] ——, "Super nested arrays: Linear sparse arrays with reduced mutual coupling—part II: High-order extensions," *IEEE Transactions on Signal Processing*, vol. 64, no. 16, pp. 4203–4216, 2016.

[11] P. P. Vaidyanathan and P. Pal, "Sparse sensing with co-prime samplers and arrays," *IEEE Transactions on Signal Processing*, vol. 59, no. 2, pp. 573–586, 2011.

[12] S. Qin, Y. D. Zhang, and M. G. Amin, "Generalized coprime array configurations for direction-of-arrival estimation," *IEEE Transactions on Signal Processing*, vol. 63, no. 6, pp. 1377–1390, 2015.

[13] S. Qin, Y. D. Zhang, M. G. Amin, and B. Himed, "DOA estimation exploiting a uniform linear array with multiple co-prime frequencies," *Signal Processing*, vol. 130, pp. 37–46, 2017.

[14] C. Zhou, Y. Gu, X. Fan, Z. Shi, G. Mao, and Y. D. Zhang, "Direction-of-arrival estimation for coprime array via virtual array interpolation," *IEEE Transactions on Signal Processing*, vol. 66, no. 22, pp. 5956–5971, 2018.

[15] C. Zhou, Y. Gu, Z. Shi, and Y. D. Zhang, "Off-grid direction-of-arrival estimation using coprime array interpolation," *IEEE Signal Processing Letters*, vol. 25, no. 11, pp. 1710–1714, 2018.

[16] J. Shi, F. Wen, Y. Liu, Z. Liu, and P. Hu, "Enhanced and generalized coprime array for direction of arrival estimation," *IEEE Transactions on Aerospace and Electronic Systems*, vol. 59, no. 2, pp. 1327–1339, 2023.

[17] Z. Zheng, W. Wang, Y. Kong, and Y. D. Zhang, "MISC array: A new sparse array design achieving increased degrees of freedom and reduced mutual coupling effect," *IEEE Transactions on Signal Processing*, vol. 67, no. 7, pp. 1728–1741, 2019.

[18] X. Sheng, D. Lu, Y. Li, and R. C. de Lamare, "Enhanced MISC-based sparse array with high udofs and low mutual coupling," *IEEE Transactions on Circuits and Systems II: Express Briefs*, vol. 71, no. 2, pp. 972–976, 2024.

[19] S. Wandale and K. Ichige, "xMISC: Improved sparse linear array via maximum inter-element spacing concept," *IEEE Signal Processing Letters*, vol. 30, pp. 1327–1331, 2023.

[20] M. G. Amin, *Sparse Arrays for Radar, Sonar, and Communications*. New York, NY: Wiley-IEEE Press, 2024.

[21] X.-G. Xia, "On estimation of multiple frequencies in undersampled complex valued waveforms," *IEEE Transactions on Signal Processing*, vol. 47, no. 12, pp. 3417–3419, 1999.

[22] X. Li, Y. Zhang, and M. G. Amin, "Multifrequency-based range estimation of RFID tags," in *Proceedings of IEEE International Conference on RFID*, 2009, pp. 147–154.

[23] S. Qin, Y. D. Zhang, M. G. Amin, and F. Gini, "Frequency diverse coprime arrays with coprime frequency offsets for multi-target localization," *IEEE Journal of Selected Topics in Signal Processing*, vol. 11, no. 2, pp. 321–335, 2017.

[24] K. V. Mishra, S. Mulleti, and Y. C. Eldar, "RaSSER: Random sparse step-frequency radar," *arXiv preprint arXiv:2004.05720*, 2020.

[25] ——, "Range-doppler decoupling and interference mitigation using cognitive random sparse stepped frequency radar," in *2020 IEEE Radar Conference (RadarConf20)*, 2020, pp. 1–6.

[26] Z. Mao, S. Liu, Y. D. Zhang, L. Han, and Y. Huang, "Joint DOA-range estimation using space-frequency virtual difference coarray," *IEEE Transactions on Signal Processing*, vol. 70, pp. 2576–2591, 2022.

[27] L. Xu, S. Sun, K. V. Mishra, and Y. D. Zhang, "Automotive FMCW radar with difference co-chirps," *IEEE Transactions on Aerospace and Electronic Systems*, vol. 59, no. 6, pp. 8145–8165, 2023.

[28] Y. D. Zhang and S. Sun, "Identical partitioning of consecutive integer set," in *Proceedings of IEEE Sensor Array and Multichannel Signal Processing Workshop (SAM)*, 2024, pp. 1–5.

[29] A. N. Namboothiri, M. W. T. S. Chowdhury, and Y. D. Zhang, "Non-overlapping identical division of integer set," in *Proceedings of Asilomar Conference on Signals, Systems, and Computers*, 2024, pp. 95–99.

[30] M. W. T. S. Chowdhury, Y. D. Zhang, and B. Himed, "Sparse radar waveform design exploiting consecutive integer set partitioning," in *Proceedings of IEEE International Radar Conference*, 2025.